

## ARTICLE OPEN



# Solar water purification with photocatalytic nanocomposite filter based on TiO<sub>2</sub> nanowires and carbon nanotubes

E. Horváth<sup>1</sup>✉, J. Gabathuler<sup>1</sup>, G. Bourdier<sup>1</sup>, E. Vidal-Revel<sup>1</sup>, M. Benthem Muñoz<sup>1</sup>, M. Gaal<sup>2</sup>, D. Grandjean<sup>2</sup>, F. Breider<sup>1,2</sup>, L. Rossi<sup>1</sup>, A. Sienkiewicz<sup>1,3</sup> and L. Forró<sup>1,4</sup>✉

Water contamination due to environmental conditions and poor waste management in certain areas of the world represents a serious problem in accessing clean and safe drinking water. This problem is especially critical in electricity-poor regions, where advanced water purification methods are absent. Here, we demonstrate that titanium dioxide nanowires (TiO<sub>2</sub>NWs)-based photocatalytic filters assisted only with sunlight can efficiently decontaminate water. Moreover, interweaving TiO<sub>2</sub>NWs with carbon nanotubes (CNTs) leads to the formation of a TiO<sub>2</sub>NWs/CNTs composite material and offers an additional water decontamination channel, that is of pasteurization with the visible part of the solar emission spectrum. Our results demonstrate that this nanoporous filter can successfully intercept various types of microbial pathogens, including bacteria and large viruses. In addition, photocatalytically generated reactive oxygen species (ROS) on the surface of the TiO<sub>2</sub>NWs/CNTs-based filter material under exposure to sunlight contribute to an efficient removal of a broad range of organic compounds and infective microbes. A pilot study also yielded encouraging results in reducing traces of drugs and pesticides in drinking water.

npj Clean Water (2022)5:10; <https://doi.org/10.1038/s41545-022-00157-2>

## INTRODUCTION

Universal access to clean and safe drinking water is essential for life. Since 1990 in emerging countries, the quality of water has remarkably improved due to economic growth and technological progress. Yet, even nowadays, numerous locations throughout the world are constantly exposed to risks of contamination and still suffer from the lack of sanitary infrastructure. According to the World Health Organization (WHO) [1], at least 1.8 billion people, mainly in rural areas, consume water that is contaminated with feces. According to the United Nations Children's Fund (UNICEF), an estimated number of 1,800 children die every day (diarrhea) because of unsafe water supply [2]. WHO reports that by 2040, a large portion of the world will endure water stress in relation to the dramatically insufficient drinking water resources. For this reason, the same source predicts a global crisis regarding universal access to clean and safe drinking water.

This problem may prove to be especially acute in countries where sanitary infrastructure is not at place or disrupted (e.g., at remote, rural or war-affected areas), as well as in electrical energy-disadvantaged communities, where running advanced purification methods is not feasible. Under such circumstances, people are forced to drink water contaminated by feces, parasites, life-threatening harmful bacteria, viruses, etc. These pathogenic species could be of various nature, like, e.g., *Escherichia Coli*, *Salmonella*, *Cryptosporidium*, or *Hepatitis A*, which could cause not only stomach pain, fever, headache, painful diarrhea and fatigue, but even death, as in the case of *Legionella Pneumophila* infection. It is then important to find a simple and efficient way to eliminate them to provide clean, safe and affordable drinking water in a cost-effective manner.

One of the possible solutions would be to make use of the photocatalytic water treatment by combining sunlight with nanoscale forms of titanium dioxide (TiO<sub>2</sub>). In fact, this approach

for water decontamination has been extensively investigated since 1985 [3–8]. TiO<sub>2</sub> is a wide-band gap semiconductor, which efficiently absorbs the ultra-violet (UV) part of the sunlight spectrum. For typical photocatalytic applications, due to their large specific surface area, the nano-sized forms of TiO<sub>2</sub>, e.g., TiO<sub>2</sub> nanoparticles (TiO<sub>2</sub>NPs) or TiO<sub>2</sub> nanowires (TiO<sub>2</sub>NWs), are of particular importance. The electron-hole pairs induced by the absorbed UV photons diffuse to the surface of TiO<sub>2</sub>NPs or TiO<sub>2</sub>NWs, where, in contact with water and oxygen molecules, reactive oxygen species (ROS) are produced. In the aquatic environment this photocatalytic mechanism generates various kinds of ROS, the most important of which are: hydroxyl radical (OH<sup>•</sup>), superoxide radical anion (O<sub>2</sub><sup>•-</sup>), hydrogen peroxide (H<sub>2</sub>O<sub>2</sub>), and singlet oxygen (<sup>1</sup>Δ<sub>g</sub>) [9]. In turn, ROS formed on the surface of photo-excited TiO<sub>2</sub>NPs, before they decay, can readily attack and react with organic contaminants and pathogens, if there are any in the immediate vicinity.

Thus, due to the high specific surface area of nano-sized photocatalytic particles, their efficient photo-generation of ROS, as well as large contact surface and direct interactions, the photocatalytic systems based on nanoparticle forms of TiO<sub>2</sub> provide a powerful disinfecting strategy against waterborne microorganisms and pathogens [10, 11]. However, despite the significant potential and many advantages of such an approach, no operational photocatalytic sunlight-driven titania-based devices have been elaborated up to date. The current situation can be explained in part by the technical complications, which are directly related to the nanoparticle form of titania. More specifically, in slurry-type reactors, after completed photocatalytic cycles, it is difficult to collect and recycle TiO<sub>2</sub>NPs (20–100 nm in size), which are dispersed in suspension containing the pollutants.

To overcome this problem, different techniques of immobilization of TiO<sub>2</sub>NPs on various types of substrates have been

<sup>1</sup>Laboratory of Physics of Complex Matter, Ecole Polytechnique Fédérale de Lausanne, Lausanne, Switzerland. <sup>2</sup>Central Environmental Laboratory, Ecole Polytechnique Fédérale de Lausanne, Lausanne, Switzerland. <sup>3</sup>ADSresonances Sàrl, CH-1028 Prévêrenge, Switzerland. <sup>4</sup>Present address: Stavropoulos Center for Complex Quantum Matter, University of Notre Dame, Indianapolis, IN, USA. ✉email: [endre.horvath@epfl.ch](mailto:endre.horvath@epfl.ch); [lforro@nd.edu](mailto:lforro@nd.edu)

developed [12, 13]. However, TiO<sub>2</sub>NPs immobilized in the form of compact thin films and porous coatings usually reveal mechanical and structural instabilities, because the powdery deposits tend to detach and fall apart exposed to the action of even weak friction and shear forces.

In this regard, here, we report the design and characterization of a highly efficient and durable photocatalytic water filter, which is based on a nanocomposite material consisting of titanium dioxide nanowires (TiO<sub>2</sub>NWs) and carbon nanotubes (CNTs).

The device has a very simple (planar) configuration, in which the contaminated water passes through a multi-layered filter material, the pathogens are trapped on the filter surface, whereas the UV component of the sunlight, being strongly absorbed by TiO<sub>2</sub>NWs, generates ROS. Therefore, in addition to the mechanical retention of pathogens, the photo-triggered ROS attack and kill diverse range of pathogenic species, including bacteria and germs, thus leading to even more efficient water decontamination. Furthermore, implementation of CNTs in the herein developed composite contributes to enhancing the photocatalytic action under exposure to sunlight [14, 15]. Especially, electrically-conducting CNTs absorb a broad spectrum of the sunlight radiation, which heats up the filter material and thus provides an additional channel for water disinfection via pasteurization [16, 17].

To further improve the photocatalytic properties of the composite filter material elaborated herein, we have also proposed to combine the TiO<sub>2</sub>NWs/CNTs composite with gold nanoparticles (AuNPs). The issue of incorporation of AuNPs into the structure of the filter material and its influence on the resulting photocatalytic properties is discussed in a more complete manner in the final part of this study (Summary).

In brief, this study reports a tailored synthetic method to prepare a solar water purifier, its basic active components, as well as its thorough characterization in terms of photo-generation of ROS—towards the removal of a wide spectrum of toxic chemicals and pathogens from drinking water.

## RESULTS AND DISCUSSION

### General concept of the TiO<sub>2</sub>NWs/CNTs nanocomposite-based water purification filter

As mentioned above, the essential building elements of the herein elaborated nanoporous photocatalytic filter material are TiO<sub>2</sub>NWs and CNTs. A simple representation of the working principle of this

TiO<sub>2</sub>NWs/CNTs nanocomposite for water filtration is shown in Fig. 1.

In particular, thanks to its nanoporous structure, the composite filter material efficiently retains waterborne microbial pathogens (a typical few of them are schematically depicted in Fig. 1a). Moreover, the filter paper decontaminates the polluted water through the action of ROS, which are photo-catalytically generated under the influence of the UV component of sunlight on the TiO<sub>2</sub>NWs surface due to their direct contact with water and oxygen molecules [18] (Fig. 1b).

When it comes to the function played by CNTs in the TiO<sub>2</sub>NWs/CNTs nanocomposite material developed by us, it is generally accepted that the presence of CNTs enhances the photocatalytic effect in two ways. Specifically, numerous reports have shown that CNTs in combination with either TiO<sub>2</sub>NPs or TiO<sub>2</sub>NWs can act as electron acceptors to more effectively separate charges photo-generated within TiO<sub>2</sub> nanostructures and thus significantly improve the photocatalytic properties of such constructs [14, 15]. In addition, the broadband absorption of solar radiation leads to heating of the filter material, thereby allowing photo-thermal disinfection of water [16, 17]. Indeed, we show that the herein elaborated combination of TiO<sub>2</sub>NWs with CNTs, gave a considerable improvement in the functioning of the filter material.

### Synthesis and structural characterization of TiO<sub>2</sub>NWs/CNTs nanocomposite

High resolution TEM images of the individual nano-structural components, that is of a single TiO<sub>2</sub>NW and a single CNT, are shown in Fig. 2a, b, respectively. For the practical implementation of numerous variants of the filter material, a large-scale production of both TiO<sub>2</sub>NWs and CNTs was developed in our laboratory. The detailed description of the large-scale synthesis routes of TiO<sub>2</sub>NWs can be found in ref. [19]. and in the U.S. patent 'Titanium oxide aerogel composites' filed by us [20].

In short, the first step of the synthesis yields titanate (H<sub>2</sub>Ti<sub>3</sub>O<sub>7</sub>) nanowires, which recrystallize into anatase TiO<sub>2</sub>NWs during the subsequent heat treatment process. While using this technological approach, in our laboratory conditions we were able to produce an amount of ~0.3–1.0 kg of TiO<sub>2</sub>NWs per day in a single synthesis cycle. However, it is worth mentioning that prospective industrial production would not be subject to such quantitative restrictions.

The mass production of CNTs was accomplished by a process of catalytic chemical vapor deposition (CVD) performed in an inclined rotary tube furnace operating in continuous mode [21].

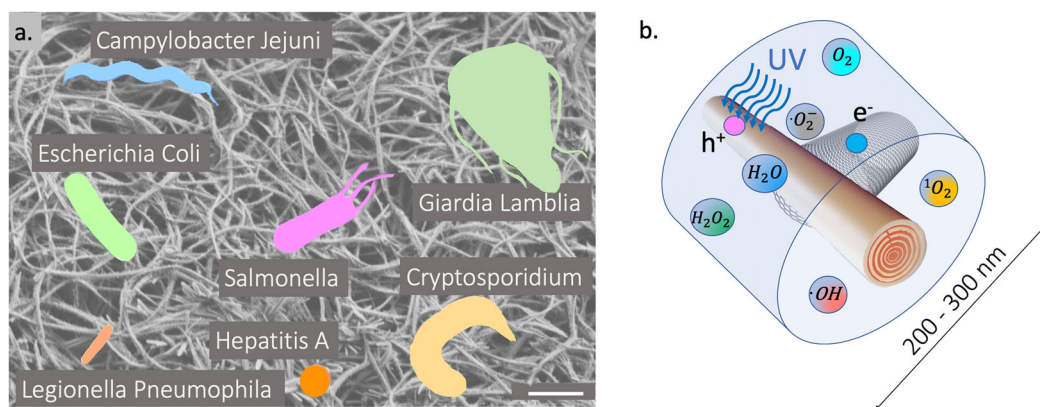


**Fig. 1 Filtering and sterilization principles.** **a** A representative selection of microorganisms, which could contaminate the drinking water. They are trapped at the surface of the TiO<sub>2</sub>NWs/CNTs composite - based filter. The sketches of the pathogens are shown on the same scale as the filter material, except for the Hepatitis A virus, the diameter of which is of 24 nm. **b** The principle of ROS generation at the surface of TiO<sub>2</sub>NWs upon UV illumination. Since the lifetime of ROS (OH<sup>•</sup>, H<sub>2</sub>O<sub>2</sub> and O<sub>2</sub><sup>•-</sup>) is short, the volume of action is also indicated. Incorporation of CNTs into the TiO<sub>2</sub>NWs/CNTs nano-construct efficiently separates electron-holes pairs photo-generated within TiO<sub>2</sub>NWs, thus reducing their recombination rate and consequently increasing the efficiency of photocatalysis. (The scalebar in a) is 1 μm).

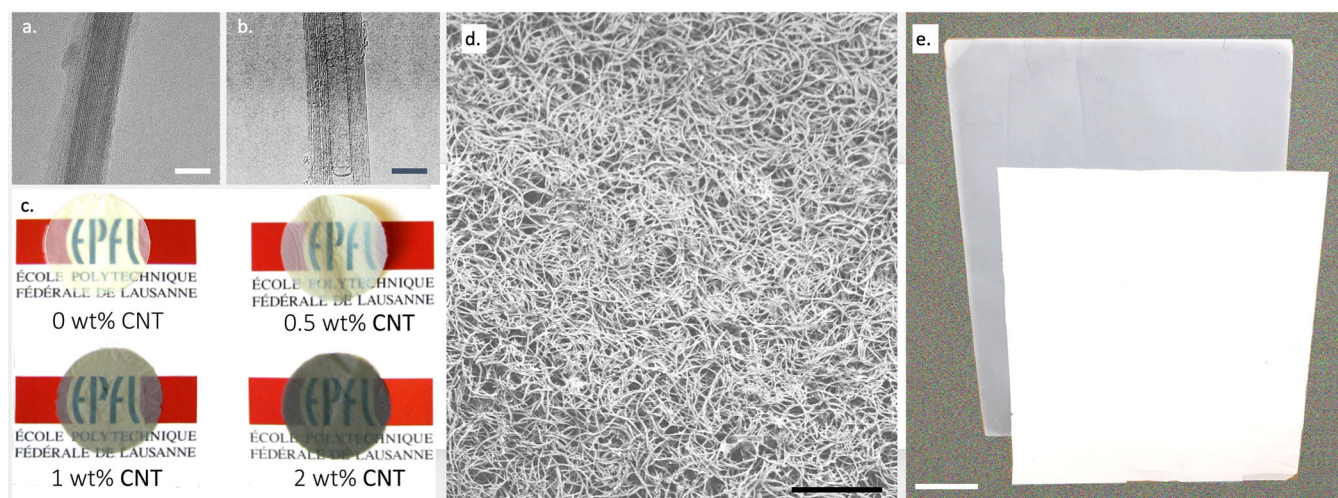


**Fig. 2** From nanowires and nanotubes to large area filter paper. **a, b** HR TEM images of the essential individual nano-structural components of the composite filter material, i.e., a single  $\text{TiO}_2\text{NW}$  and a single multiwalled CNT, respectively. The length of both nanoelements can reach several micrometers (The scalebars are 10 nm); **(c)** Photos of selected samples of  $\text{TiO}_2\text{NWs}$ -based filter paper with various wt% contents of CNTs, which alters their transparency (the diameter of the filter paper disc is of 20 mm); **d** Characteristic SEM image of the filter paper (The scalebar is 5  $\mu\text{m}$  in 5b), **(e)** Photo of large area filter papers synthesized from pure  $\text{TiO}_2\text{NWs}$  (front) and containing 1 wt% content of CNTs (grayish). (The scalebar is 10 cm).

As explained in Methods, the overnight synthesis produced  $\sim 1.2$  kg of CNTs.

The above-described high-efficiency synthesis processes of both nano-structural components, i.e.,  $\text{TiO}_2\text{NWs}$  and CNTs, allowed us to fabricate photocatalytic filtering papers with large surface areas. To this end,  $\text{TiO}_2\text{NWs}$  and CNTs were mixed in different proportions in order to optimize the filter's performance in terms of water sterilization. Subsequently, the corresponding mixtures were processed by doctor blading into films of various thicknesses, ranging from 2  $\mu\text{m}$  up to 300  $\mu\text{m}$ . The thin layers obtained this way could easily be detached from the hydrophobic support material. After air drying at 120  $^\circ\text{C}$  and calcination in vacuum at 600  $^\circ\text{C}$ , a phase transformation from titanate to anatase was achieved. It is worth mentioning here that the calcination process fuses  $\text{TiO}_2\text{NWs}$  together, thus leading to the formation of a thin filtering membrane with a tightly compact structure, which, in normal use (i.e., under standard volume flow-rates), does not release nano-structural ingredients. In short, the technology developed herein made it possible to produce freestanding, flexible thin filtering papers with large surfaces, which, depending on their thickness, could even be transparent. Examples of such thin disc-shaped filtering membranes (50  $\mu\text{m}$  thick, 20 mm in diameter), with various wt% contents of CNTs, are shown in Fig. 2c.

The surface appearance of the filter is shown in an SEM image in Fig. 2d, while the large surface area ( $\sim 0.3$   $\text{m}^2$ ), self-standing filter papers used for the fabrication of the solar-thermal water purification prototype are displayed in Fig. 2e, for pure  $\text{TiO}_2\text{NWs}$  (white) and with 1 wt% content of CNTs (grayish).

### Design of a prototype of a photo-catalytic filter and characterization of its flow-rate and photo-thermal properties

The large area filter paper made it possible to fabricate a prototype of a solar-thermal water purification system (Fig. 3a). For this purpose, a freestanding 30  $\mu\text{m}$  thick filter paper with dimensions of 37.5 cm  $\times$  28.0 cm was positioned and fixed between two 1.5 mm thick borosilicate glass windows. In our design, borosilicate glass was chosen because of its low absorbance in the UV range. The water inlet and outlet were placed on the opposite diagonal sides of the device (Fig. 3b). The stacked assembly was sealed and mechanically secured by a rectangular aluminum frame. For receiving the highest photon

flux, the sun-facing surface area of  $\sim 0.1$   $\text{m}^2$  could easily be positioned at an optimal angle ( $\theta$ ) with respect to solar radiation. The total internal volume of the device was estimated to be of  $200 \pm 50$  ml.

The possibility of efficient heating of the influent water due to the photo-thermal effect is also an important attribute of the developed filtering device. In our opinion, this functional property is related to the presence of CNTs in the structure of the filtering layer. Absorbing a broad spectrum of sunlight, these carbon nanowires with a metallic character heat up the filter and water in its immediate vicinity, thus enabling sterilization by elevated temperatures. In particular, temperatures of the order of 50  $^\circ\text{C}$  could be attained inside the prototype after approximately 1 h. of exposure to solar radiation (during a sunny afternoon on June 11th in Lausanne, Switzerland). To illustrate the thermal characteristics of the prototype, temperature was measured with both a thermocouple (on the surface of the device) and an infrared camera. The corresponding time dependencies of the device temperature exposed to the sun radiation for about 60 min are shown in Fig. 3c. It is worth mentioning that no forced water flow was used in this experiment. Therefore, the outcome of this experiment reflects the maximum potential temperature that the device can attain under similar meteorological conditions.

An important parameter of the filtering system is its flow-rate ( $Q$ ), defined as the purified water volume ( $V$ ) passing through the device per unit time ( $t$ ), i.e.,  $Q = V/t$ . This volume flow-rate is usually described by Darcy's law [22], which states that the fluid flow-rate through a filtration device is directly proportional to the corresponding pressure gradient, that is:  $Q = \kappa A \Delta p / \mu L$  where  $Q$  [ $\text{m}^3 \cdot \text{s}^{-1}$ ] is the volume flow-rate,  $\kappa$  [ $\text{m}^2$ ] is the permeability of the medium,  $A$  [ $\text{m}^2$ ] is the filter area,  $\Delta p$  [ $\text{Pa}$ ] is the pressure drop across the filter membrane of thickness  $L$  [ $\text{m}$ ], and  $\mu$  [ $\text{Pa} \cdot \text{s}$ ] is the viscosity of the fluid.

The drop of pressure across the filtering device can be varied by changing the vertical separation between the polluted water tank and the filter outlet, in accordance to the Pascal's law:  $\Delta p = \rho gh$ , where  $g$  is the gravitational constant,  $\rho$  stands for the fluid density and  $h$  abbreviates the vertical separation distance (height). For the meaning of the symbols see Fig. 3b. The measured dependencies of the water volume flowing through the device as a function of time for three values of  $h$ : 75, 120 and 160 cm is shown in Fig. 3d. Qualitatively, the Darcy's law is satisfied, although for higher

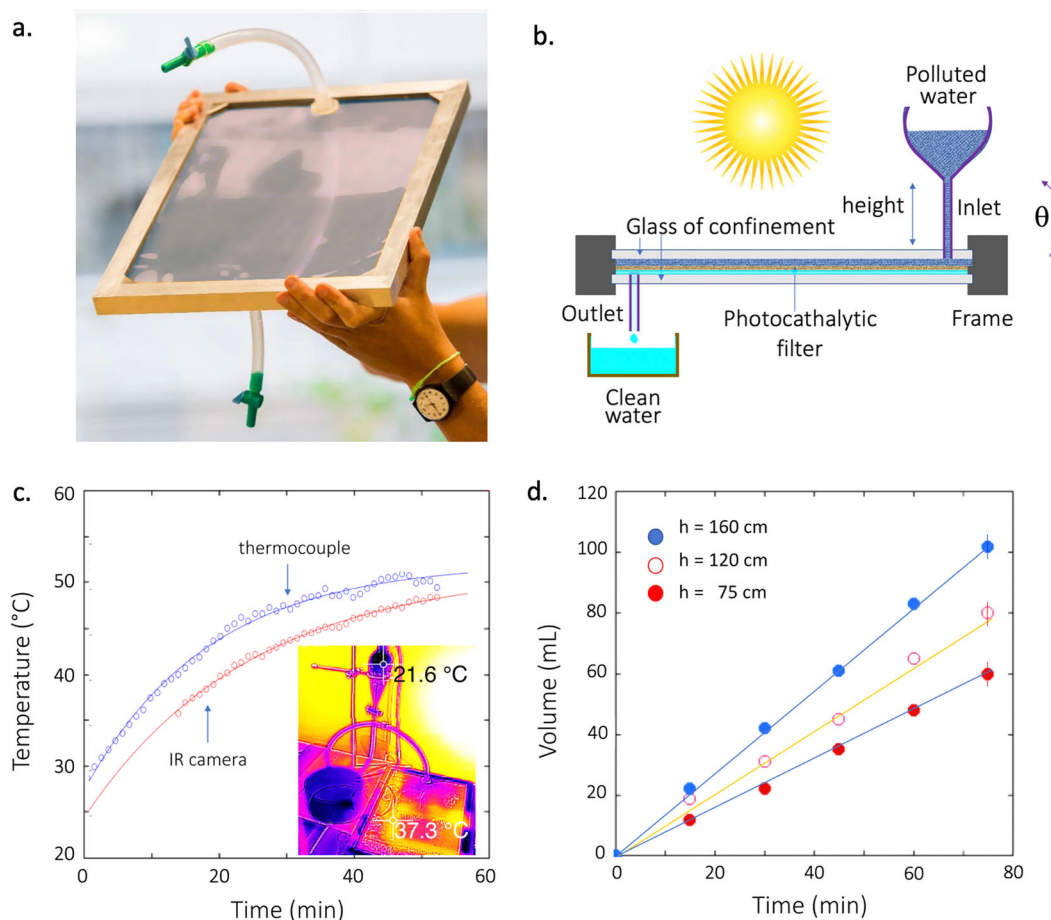


**Fig. 3 The prototype of a solar-thermal water filter and its characterization.** **a** Photograph of the device (with a visible random mirror image of the surroundings on the outer glass surface of the filter) and **(b)** the sketch of the cross-section of the prototype. The flow-rate through the device depends on the water pressure through the difference in elevation levels between the contaminated water tank and the clean water outlet (symbolically marked as height,  $h$ ). The orientation of the device can easily be adjusted to an optimal angle ( $\theta$ ) with respect to solar radiation; **(c)** Temperature of the solar-thermal device when exposed to the sun. The limit temperatures are of 52.2 and 52.9°C for the fit curves for the infrared camera and for the thermocouple, respectively. The inset shows the infrared image of the prototype at one temperature point during its exposure to sunlight; **(d)** Purified water volume flowing through the device as a function of time for three values of  $h$ : 75, 120 and 160 cm. The rectilinear slopes of the plots confirm the dependence of the volume flow-rate on  $h$  according to the Pascal's law.

$h$  values, there might be some pressure loss, since  $V$  versus  $h$  is not strictly linear. As can be seen, even this small surface area filter can supply *ca.* 2.0 liters of decontaminated water per day.

#### Overview of experimental techniques characterizing the photo-catalytic performance of the filter

The photo-catalytic efficiency of the filtering composite material prepared in this work was checked for a broad spectrum of potential targets, ranging from small molecular compounds to bacteria. In particular, for characterization of the photocatalytic generation of ROS the following methods were implemented: electron spin resonance (ESR), optical spectroscopy and standard microbiological bacteria survival tests. In addition, for measuring the variation of minute concentrations of molecules, such as drugs and pesticides in water, mass spectrometry (MS) coupled with high-performance liquid chromatography (HPLC) was applied.

#### Photo-catalytic generation of ROS tracked by ESR test based on TEMPOL decay

To confirm the efficient photocatalytic generation of ROS in an aqueous environment by the  $\text{TiO}_2\text{NWs/CNTs}$ -based filtering composite material, ESR in combination with spin-trapping

was employed. Specifically, a stable nitroxide radical, 4-Hydroxy-2,2,6,6-tetramethylpiperidine-1-oxyl (TEMPOL), was used as a target molecule for the photo-generated ROS, i.e.,  $\text{OH}^\cdot$  and  $\text{O}_2^{\cdot-}$  radicals [20, 23]. The ESR-active TEMPOL is a water-soluble antioxidant, which reportedly acts as a superoxide dismutase (SOD) mimicking agent [24, 25].

The reactive pathways of TEMPOL with ROS have been reported to introduce structural changes at the 1- and 4-positions of this nitroxide molecule, for  $\text{O}_2^{\cdot-}$  and  $\text{OH}^\cdot$  radicals, respectively [26]. Acting in concert, these structural changes induce the decay of the ESR-active TEMPOL, as well as lead to the concurrent formation of another ESR-active radical, the 4-oxo-TEMPO (TEMPONE).

In aqueous solutions, both TEMPOL and TEMPONE reveal easily detectable ESR spectra, which are characteristic for NO-centered radicals bearing one unpaired electron ( $S = 1/2$ ). Specifically, the corresponding ESR signals consist of three well-resolved features resulting from the  $^{14}\text{N}$  atom-related hyperfine splitting ( $I = 1$ ). Due to the differences in the hyperfine splitting constants,  $A^{14}\text{N}$ , and the spectroscopic  $g$ -factors values, being of 17.1 G/2.0057 and 16.1 G/2.0056, for TEMPOL and TEMPONE, respectively, these two nitroxide radicals can be very easily distinguished [27].

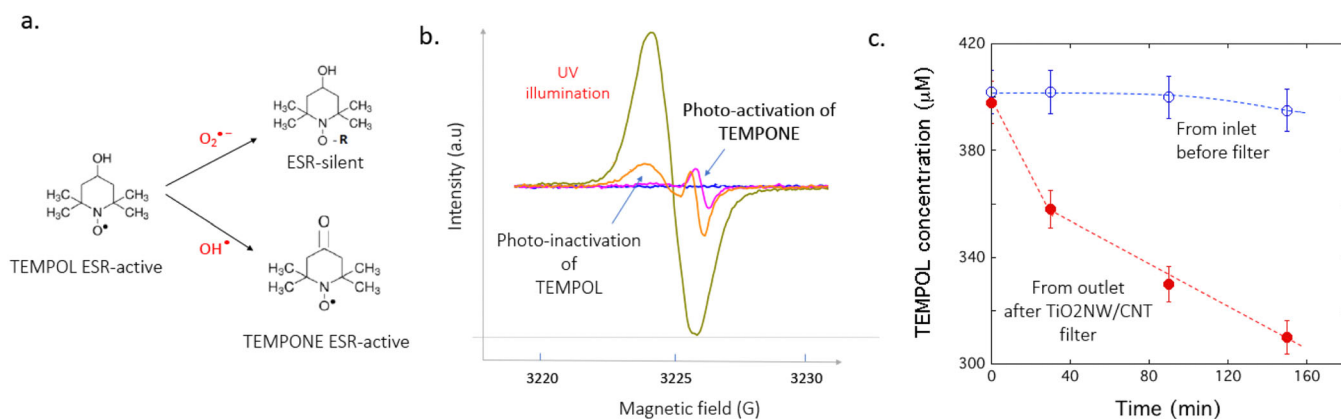


**Fig. 4 ESR detection of ROS generation.** **a** Principle of oxidative stress evaluation with using a stable nitroxide radical, TEMPOL. The reducing/oxidative action of the photo-generated ROS deprives the TEMPOL molecule of spin and makes it ESR-silent. Through a competing process, the OH<sup>•</sup> radical attacks the TEMPOL molecule at the 4-position and converts it to another ESR-active nitroxide, TEMPONE. **b** The ROS-induced progressive decay of the ESR signal of TEMPOL is accompanied by the occurrence of the ESR signal of TEMPONE, as observed over 120 min time under exposure to UV-A. **c** Time-evolutions of the ESR signal intensities of TEMPOL monitored at the entrance and outlet of the TiO<sub>2</sub>NWs/CNTs—based photocatalytic filter.

The principle of the ESR experiment allowing for an indirect detection and evaluation of photo-catalyzed ROS, with using TEMPOL as a target molecule, is shown schematically in Fig. 4a. In particular, the diagram in this figure depicts the two most important reaction pathways related to the attack of O<sub>2</sub><sup>•-</sup> and OH<sup>•</sup> radicals on TEMPOL, thus leading to the ESR-silent TEMPOL-hydroxylamine (TEMPOL-H) and the ESR-active TEMPONE, respectively.

Considering the course of the ESR signals of TEMPOL and TEMPONE as a function of time, it seems clear that their time-evolutions confirm the presence of ROS, but with divergent dependencies. In particular, as a function of time, the ESR signal intensities of TEMPOL and TEMPONE, gradually decay and increase, respectively.

Typical results of ROS detection by means of ESR using TEMPOL as a molecular target are shown in Fig. 4b. Specifically, it can be seen that for the generation of ROS by TiO<sub>2</sub>-based photo-catalyst, after a prolonged illumination with UV-A light, the ESR signals of TEMPOL and TEMPONE clearly decrease and increase, respectively. Note that only the low-field hyperfine components of the ESR spectra of TEMPOL and TEMPONE are shown in Fig. 4b.

During this experiment, both sides of the filtering device were illuminated by a UV-A light source, which was operating at the wavelength of 367 nm with the power intensity of ~1–3 mW/cm<sup>2</sup>.

To check the efficiency of the prototype in photo-generation of ROS when exposed to sunlight, the samples for ESR measurements were taken regularly over an extended period of time from the inlet and outlet of the filter (see Fig. 3b). Before starting the experiment, the upper tank of the device was filled with the volume of two liters of 400 μM aqueous solution of TEMPOL.

Changes in the intensities of the ESR spectra during the filter's exposure to sunlight were assessed by comparing the double integrals of the corresponding ESR signals acquired sequentially as a function of time (for more details see METHODS).

The corresponding plots of the ESR signal intensities monitored at the entrance and outlet of the prototype filtering device over ~2.5-h. period of exposure to sunlight, during the sunny early afternoon of April 6<sup>th</sup> in Lausanne, Switzerland, are displayed in Fig. 4c. As shown, the ESR signal intensity of TEMPOL decreases strongly with time after its passage through the filter, which is the consequence of the ROS-induced damage. It is worth mentioning that the simultaneous creation of the ESR-active TEMPONE compensates to a relatively small extent the herein observed overwhelming decay of the paramagnetic TEMPOL. In fact, as mentioned before, both these processes confirm the divergent

mechanisms of ROS-mediated actions on the same target molecule (TEMPOL). Thus, this observation validates the final conclusion that TiO<sub>2</sub>NWs/CNTs-based composite is very efficient in generating ROS and the accompanying oxidative stress on its surface.

#### Photodegradation of Methyl orange—a UV–VIS assay

The colorful dye, methyl orange (C<sub>14</sub>H<sub>14</sub>N<sub>3</sub>NaO<sub>3</sub>S, abbreviated as MO) is often used as a model organic pollutant for evaluation of the ROS generation efficiency and the oxidative stress conditions in various environments [28–30]. The usefulness of MO for this type or research is due to the fact that the ROS-mediated damage to MO reduces its strong absorption band at 464 nm. In particular, under the influence of photo-oxidative stress, the MO molecules undergo the successive stages of hydroxylation, demethylation and oxidation, which result in photo-bleaching and, ultimately, complete loss of color. The corresponding changes in the molecular structure of the dye can be associated to its concentration and easily be monitored by the changes in the dye's absorbance (*A*), according to the Beer–Lambert law expressed as  $A = \epsilon lc$ , where  $\epsilon$  is the molar attenuation coefficient, *l* is the optical path, and *c* is the MO concentration.

In this experiment, MO dissolved in distilled water (Millipore), with an initial concentration *c*<sub>0</sub> = 20 mg/mL was poured into Petri dishes (90 mm in diameter and 15 mm height) containing the test samples in the form of discs (50 mm in diameter) at their bottom. For the purpose of exposure to UVA light, a UV spot light source, LC-8 Lightingcure™ ( $\lambda_{\text{exc}} = 365 \text{ nm}$ , 16 mW/cm<sup>2</sup>, from Hamamatsu Photonics (Japan), was used. The photocatalytic activity of the herein developed composite material based on TiO<sub>2</sub>NWs/CNTs was tested, as well as two reference materials: a commercial standard photocatalyst, TiO<sub>2</sub>NPs (Degussa P25), having similar specific surface area (~40 m<sup>2</sup>/g), and a nano-structured aluminum oxide (Al<sub>2</sub>O<sub>3</sub>).

The photodegradation of the dye and the corresponding changes in its concentration were monitored by measuring the characteristic MO absorbance peak at 464 nm with a UV–VIS spectrophotometer, Varian Cary 50, Agilent (USA). In order to obtain the time dependencies, small aliquots (2.5 mL) were taken every 10 min from Petri dishes and transferred to the cuvettes of the UV–VIS spectrophotometer.

All these test measurements were performed under static conditions, *i.e.*, without flow or mixing/stirring the MO solution in

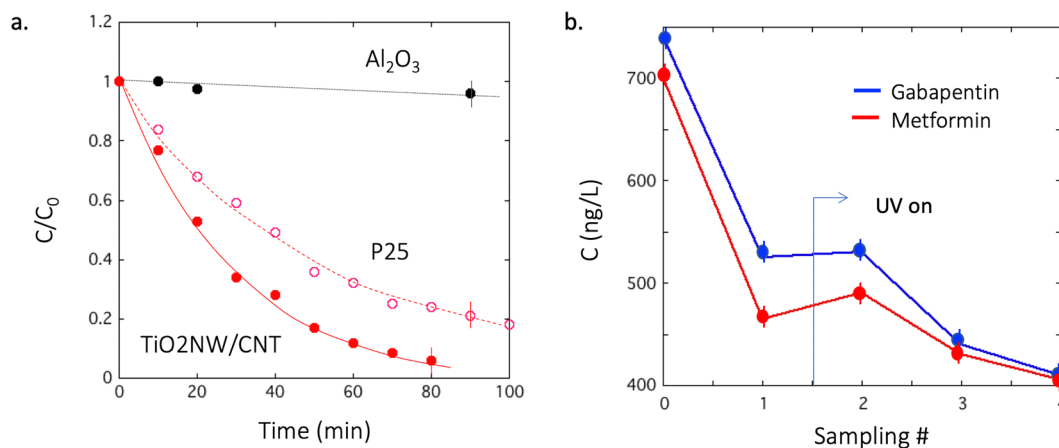


**Fig. 5 Photodegradation of methyl orange (MO) and of micropollutants in the presence of the TiO<sub>2</sub>NWs/CNTs.** **a** The normalized concentration ( $C/C_0$ ) of MO versus UVA illumination time in the presence of the TiO<sub>2</sub>NWs/CNTs filter (red dots). The herein monitored MO degradation efficiency was compared to that of P25 TiO<sub>2</sub>NPs (Degussa) deposited on an anodic aluminum oxide (Al<sub>2</sub>O<sub>3</sub>) membrane (gray circles) and also compared to the efficiency of the same anodic Al<sub>2</sub>O<sub>3</sub> membrane without any coverage (black dots); For illumination with UVA, a UV spot light source ( $\lambda_{\text{exc}} = 365 \text{ nm}$ ,  $16 \text{ mW/cm}^2$ ), model LC-8 Lightingcure™ (Hamamatsu Photonics, Japan) was implemented; **(b)** After the first passage through the TiO<sub>2</sub>NWs/CNTs photocatalytic filter, both micropollutants slightly desorb, which coincides with starting of UV-A illumination (due to thermal desorption). For subsequent passages, however, the photo-generated ROS take over and destroy these harmful molecules.

Petri dishes. As shown in Fig. 5a, the filter paper elaborated herein is twice as efficient as the P25 itself.

It has been shown that CNTs in combination with other semiconducting nanomaterials, such as, e.g., TiO<sub>2</sub>NPs or zinc oxide NPs (ZnONPs), substantially reinforce the photo-catalytic efficiency of composite photo-catalytic materials [31]. In particular, it has been demonstrated that the presence of CNTs in these composite materials enhances their photocatalytic efficiencies through increased total active surface area and electrical conductivity [32]. Therefore, in the presence of CNTs, these contributions increase lifetimes of the photo-generated electron-hole pairs generated by semiconducting nanomaterials, thus improving their overall photo-catalytic performance [16].

### Degradation of micropollutants

Micropollutants, such as drug residues, pesticides, maintenance products, hormones, or cosmetics, contaminate drinking water worldwide and may have a long-term toxic effect on living organisms and the ecosystem [33–35]. In this regard, we also examined whether our photocatalytic filter was able to reduce their concentrations. To this end, the Central Environmental Laboratory of EPFL prepared a “cocktail” of nine micropollutants (five drugs, three pesticides and one maintenance product: atrazin, carbamazepin, diclofenac, mecoprop, metolachlor, bezotriazol, lomeprol, gabapentin, metformin). They were dissolved in 5 L of distilled water, representing a concentration of hundreds nanograms per liter (ng/L). After each passage through the filter, the micropollutants were separated by high-performance liquid chromatography (HPLC), and various bands were analyzed with mass spectrometry (MS). Figure 5b shows the results of the successful removal of two selected micropollutants, i.e., gabapentin (painkiller) and metformin (drug for diabetes).

The first passage performed in the dark (sampling 1) showed a global decrease in concentrations of both gabapentin (blue trace) and metformin (red trace), that can be attributed to the adsorption of a certain part of the compounds on the filter surface. Specifically, as can be seen in Fig. Fig. 5b, the concentrations of both compounds decreased by ~25% during the 1st sample run. This downward trend in the concentration of both chemicals was partially stopped during the 2nd sampling period. The herein observed inhibition of the filtration process and the accompanying

slight increase in the concentration of both chemicals may be related to thermal desorption. Actually, it also coincides with the beginning of exposure of the filter to illumination with UVA light (365 nm,  $1 \div 3 \text{ mW/cm}^2$ ). However, during the next sampling runs (samplings 3 and 4), a small drop in concentrations of both micropollutants was observed, what can be attributed to the ROS-mediated photo-decomposition (see Fig. 5b). This small, though measurable change might be due to very low concentrations of gabapentin and metformin, and their relatively short residence time under flow conditions within the volume where ROS are photo-generated (see Fig. 1b). An additional argument supporting this rather minor effect of micropollutant photodegradation can also be related to the very low power density of the incident UVA radiation in this experiment. Although the observed decrease in concentration is slight, it nevertheless suggests the potential of the herein developed TiO<sub>2</sub>NWs/CNTs-based photocatalytic filter for the removal of micropollutants from water.

### Microbiological tests of the mechanical removal and photo-oxidative sanitation of waterborne pathogens

The capability of the device to filter out germs from water was verified using the Colilert and Quanti-Tray method [36, 37]. This is a standard method to indicate the sanitary quality of water, e.g., the evidence of fecal contamination with coliform bacteria, with special emphasis on *E. coli*. In practical application of this method, the enzymatic activity of coliform bacteria metabolizes two nutrient-indicating molecules, i.e., ortho-nitrophenyl- $\beta$ -D-galactopyranoside (ONPG) and 4-methyl-umbelliferyl- $\beta$ -D-glucuronide (MUG). More specifically, in the general case of the presence of coliform group bacteria, the metabolized ONPG turns the colorless water into yellow, whereas in the specific case of the presence of *E. coli*, MUG renders the aqueous milieu fluorescent upon UV illumination. In this approach, the enumeration of coliforms and *E. coli* in water samples is performed using so-called colony-forming units (CFU).

The tested water sample was taken from the river La Chamberonne (passing nearby the laboratory). Prior to performing the contamination test, an aliquot of 1 ml of this water was 100 times diluted with distilled water. Next, before and after passing through the filter, the water was mixed with the Colilert reagent, poured into Quanti-trays and incubated at 35 °C for 24 h. The

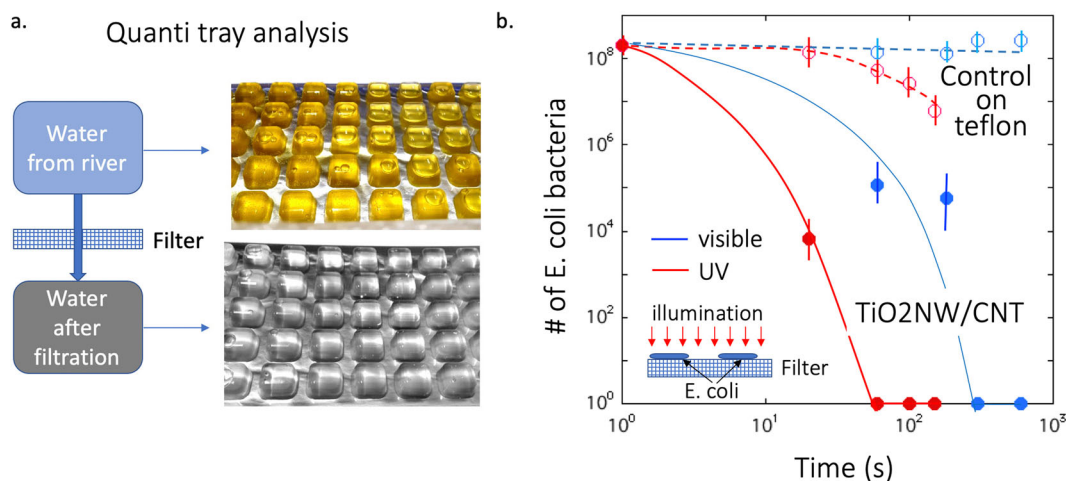


**Fig. 6** Quanti-tray analysis of the efficiency of the filtration of the device and the *E. coli* bacteria survival. **a** The presence of coliform bacteria in the 100 times diluted river water is indicated by the yellow color of the Quanti-tray (upper part of the image), whereas the colorless Quanti-tray confirms that no bacteria passed through the TiO<sub>2</sub>NWs/CNTs filter (lower part of the image); **(b)** The bacterial inactivation performance of the TiO<sub>2</sub>NWs/CNTs filter upon UVA and visible light illumination as compared to the control surface of the humid Teflon filter. After 30 sec of illumination with UVA light and after more than 300 sec when exposed to visible light, the concentrations of bacteria are below the detection limit. Inset: schematic representation of the experiment showing the location of the bacteria-containing spots on the filter's surface.

results are shown in Fig. 6a. The Quanti-tray containing the untreated water turned completely yellow and became also fluorescent under UV light (not shown), while the Quanti-tray with the filtered solution did not change color. Moreover, as can be seen in the upper portion of Fig. 6a, all the cells of the Quanti-tray containing the untreated water are yellow, thus confirming the contamination with coliform bacteria at the level higher than 200 CFU/100 ml. In contrast, the assessment of the Quanti-tray containing the treated water (lower portion of Fig. 6a), points to the contamination level well below 1 CFU/100 ml.

Thus, the Colilert and Quanti-Tray procedure confirmed the efficiency of the TiO<sub>2</sub>NWs/CNTs-composite-based filter for the mechanical removal of waterborne pathogens, including *E. coli* bacteria. This high filtration efficiency can be attributed to the small cut-off size of the filter pores (<1  $\mu$ m).

Below we show that apart from the mechanical retention of pathogens, the photocatalytic properties of the herein developed filter material also allow for their complete deactivation. To this end, a second microbiological test was performed. Specifically, we employed the conventional plate count technique, in which, similarly to the previously discussed Colilert and Quanti-Tray test, CFU units are taken into account to estimate the number of viable microorganisms in the sample [37].

The *E. coli* bacteria survival was measured under three conditions: (i) deposited on TiO<sub>2</sub>NWs/CNTs filter and illuminated with UV light (at 365 nm with power density of 16 mW/cm<sup>2</sup>), for time intervals of 20, 60, 100 and 180 sec; (ii) deposited on the same filter, but illuminated with daily sun light extended up to 600 sec; and (iii) deposited on Teflon substrate, illuminated by the UV and visible lights for the corresponding time intervals - as control measurement. In all cases, the starting *E. coli* concentration was  $2 \times 10^8$  CFU/mL.

From the suspensions prepared that way, 5- $\mu$ L aliquots were taken, dropped on the filter surface and exposed to illumination with UVA light. After each illumination run, the filter fragments were placed in Eppendorf tubes containing physiological salt and then rinsed for 60 min. This treatment allowed to the dead *E. coli* to be removed and to enter the survived cells back into solution. Next, serial dilutions were prepared from the solution containing cells and 10  $\mu$ L aliquots of each dilution were spread onto cultivation agar in Petri dishes. Subsequently, they were incubated at 37  $^{\circ}$ C for 24 h. The enumeration of bacteria per mL (CFU/mL)

was extrapolated from the colonies counted at the appropriate spots for TiO<sub>2</sub>NWs filter, and the survival rate could be established. The results shown in Fig. 6b superbly demonstrate the antibacterial activity of the TiO<sub>2</sub>NW/CNTs filter. Already, after 60 sec of UVA light exposure the number of survived bacteria drops below the detection limit (red trace in Fig. 6b). Even after exposure for 30 sec to UVA light, the damaged bacteria could be noticed in the SEM image (not shown). A direct impact of high energy UV photons can damage the *E. coli* bacteria as shown in the control experiment on the wet Teflon filter surface, but the corresponding decrease in their number is non-comparable with that of the TiO<sub>2</sub>NWs-based photocatalytic filter.

It is also worth mentioning that in the experiment described above, the time scale in which *E. coli* inactivation occurred was much shorter than for any other tests of light-dependent oxidative stress conducted herein. The rapid photo-inactivation of *E. coli* observed in this experiment can be attributed to the fact that the bacteria were trapped on the filter surface, thus being in the immediate range of ROS photo-generated by immobilized photocatalyst particles. In addition, the entire experiment was carried out under static conditions (without water flow). Therefore, the photo-catalytically induced ROS, before their disappearance, had a better chance of reaching the bacteria. This is in contrast to other experiments, in which photodegradation of waterborne chemical compounds, such as TEMPOL or MO, was observed under flow conditions.

The apparent differences in photo-deactivation rates of adsorbed bacteria and water-soluble chemicals can then be associated to the limited volume of action of ROS generated mainly at the filter surface. Specifically, both the small volume of the direct ROS-mediated deactivation (symbolically represented by the bluish cylinder in Fig. 1b) and dynamic conditions of water flow led to the observed reduction in photocatalytic deactivation efficiency of waterborne chemicals.

Furthermore, another interesting observation is the fact that that exposure only to sunlight exerts a profound sterilizing impact and significantly eliminates *E. coli* bacteria. This sterilizing effect is related, in part, to the UV component of the sunlight spectrum, which induces photocatalytic damage to bacteria, as well as to pasteurization due to the increased temperature of the filter material containing CNTs in its structure (see Fig. 3d). Regardless of the contributions of the above-mentioned mechanisms, the

photo-thermal water filter developed in this work seems to be an interesting proposition for large-scale applications, allowing for effective water purification in the absence of specific infrastructures. The device, using solely sunlight, exerts a sterilizing effect by destroying microbial pathogens, such as bacteria or even viruses, thus rendering the polluted water safe and drinkable.

## SUMMARY

We have reported a simple approach to filter and purify water, which is based on the herein developed thermo-photocatalytic composite material, TiO<sub>2</sub>NWs/CNTs, and is using solely sunlight as a source of energy. The filter can efficiently entrap, degrade and eliminate waterborne pathogens, including bacteria, viruses and worms. Furthermore, it has also proven efficiency in photocatalytic decomposition and neutralization of waterborne organic micro-pollutants, such as drugs, pesticides and detergents.

In the filtering device constructed in this work, the sunlight-mediated disinfection of waterborne pathogens occurs due to the combined action of photo-generated ROS and thermal pasteurization, i.e., the respective contributions of photocatalytic properties of TiO<sub>2</sub>NWs and photo-thermal input of CNTs, resulting from their strong absorption in broad optical spectral range.

A small prototype of the water-filtering device with surface of 0.3 m<sup>2</sup> can supply 2 L/day of decontaminated water, which could be easily scaled up by increasing the filter surface. The great advantage of this device is that it is cost-effective, thermally stable, chemically inert, and capable of promoting oxidation of organic compounds via photo-catalytic generation of ROS. We believe that

this simple method could be a good solution for drinkable water-stressed areas.

As an outlook, to further improve the photocatalytic properties of the composite filtering material elaborated in this work, we also propose a few of possible improvements. The first could be the incorporation of gold nanoparticles (AuNPs) into the TiO<sub>2</sub>NWs/CNTs-based composite fabric, as shown in Fig. 7a, b. In this regard, earlier studies have shown that AuNPs exhibit enhanced photon absorption properties and can be used to efficiently generate local heating upon illumination through photo-induced resonant plasmons [38]. Therefore, composites consisting of the photo-active TiO<sub>2</sub> and AuNPs can be conveniently employed as plasmonic photocatalysts, enabling a number of important reactions to occur with high efficiency and under minimal light exposure [39–41]. Although the exact underlying mechanisms are still not well understood, this direction of improvement of the composite material seems to be promising. In particular, the expected improvement in photocatalytic composite material also incorporating AuNPs is related to the plasmonic effect, which works for the whole spectral range of sunlight.

A second route for improvement could be the surface structuring of the filter, in order to better trap and conduct the incident light into the bulk of the material, since, as mentioned before, both ROS generation and the resulting water pasteurization are proportional to the illuminated volume. In general, the question of more efficient light trapping is very vivid in photovoltaics in order to improve the light-matter interaction within the device's photo-active layer and thus to enhance the solar cell efficiency. One way of achieving this is through

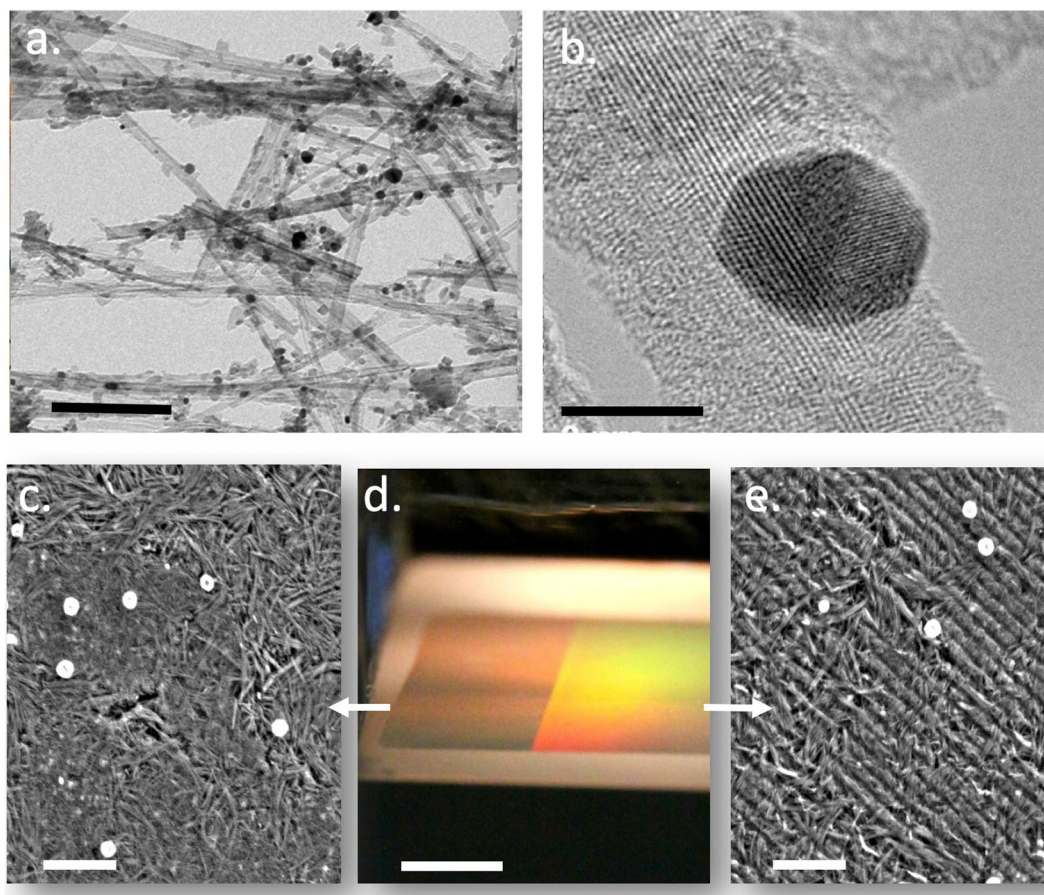


**Fig. 7 Strategies for the filter improvement by AuNPs and surface texturing.** **a** TEM images of a large assembly of the TiO<sub>2</sub>NWs/AuNPs composite (the scalebar is 200 nm), and **(b)** Enlarged image fragment selected from the image shown in **(a)** (the scalebar is 5 nm); **(c** and **e)** SEM images of the filter material without and with surface structuring, respectively (the scalebar is 2 μm). **d** Two distinctly different optical responses upon visible light illumination of non-structured (left) and structured (right) versions of the filter material (the scalebar is 10 mm).

elaboration of periodic light trapping structures. Recently, numerous such structures have been developed, including nanowires [42], nanoparticles [43], gratings [44, 45], and many more. In particular, gratings could be designed to diffract the incident light at the TiO<sub>2</sub>-air interface at angles bigger than the critical angle (depending on the grating periodicity), so that most of the potentially scattered or reflected energy could be returned to the photo-active filter layer. It has previously been shown that such surface structuring results in an effective enhancement of the optical path length and better light absorption [45].

In this regard, in Fig. 7c–e, we show that it is possible to fabricate the TiO<sub>2</sub>NWs/CNTs filter to have a grating pattern structure on its surface. Specifically, the SEM images of the as-deposited filter on a flat and lithography-modified substrate surfaces are shown in Fig. 7c, e, respectively. The grating pattern structure can easily be recognized on the surface of the filter material deposited on the lithography-engineered substrate. Moreover, as shown in Fig. 7d, these two surfaces have distinctly different optical responses, due to the enhanced light interference on the surface with the grating pattern.

Further optimization of structuring of the filter surface as well as exploration of its advantageous properties are the subjects of forthcoming studies related to the TiO<sub>2</sub>NWs/CNTs filter material.

## METHODS

### Synthesis of TiO<sub>2</sub>NWs

TiO<sub>2</sub> nano-powder with size distribution of 20–50 nm (Nanoshell LLC) was dissolved in a base solution of NaOH (Merck), and heated up to 70 °C and exposed to turbulent mixing. In a time-window of 1–24 h a high fraction of mesoporous titanates was formed with a jelly-like appearance. By centrifugation the (H<sub>2</sub>Ti<sub>3</sub>O<sub>7</sub>) NWs were separated from the reaction residues and transformed into anatase TiO<sub>2</sub>NWs by heat treatment at 600 °C (ref. [20]). The specific surface of TiO<sub>2</sub>NWs is in the 150 m<sup>2</sup>/g range.

### Synthesis of CNTs

The continuous production method of CNTs implemented in this work was based on chemical vapor deposition (CVD) performed in an inclined rotary tube furnace [21]. This approach overcomes the limited capacity and scalability of more frequently used fixed bed reactors [46, 47]. The furnace used here was equipped with a quartz tube with a diameter of 80 mm. During the CVD deposition process, the catalyst (bimetallic Fe<sub>2</sub>Ni catalytic particles on CaCO<sub>3</sub> supporter) was continuously introduced into the reaction tube with an endless screw placed at the end of the catalyst container. Acetylene and argon were fluxed at 10 L/h and 80 L/h, respectively. The material was purified by dissolving the catalyst and the support in a 1.5 M hydrochloric acid. Subsequently, MWCNTs were filtered, washed with distilled water, and dried at 120 °C overnight. A production rate of about 1.2 kg per day was achieved. The specific surface of CNTs 700 m<sup>2</sup>/g range.

### Mechanical filtration

The mean pore size distribution of the filters was characterized by polystyrene dispersion of 1.97 μm, 870 nm, 530 nm and 110 nm particles of concentration of 13.7 mg/L, which were passed through the filter. Due to intrinsic absorbance and the light scattering of polymer colloid particles, the dispersion has a characteristic absorbance spectrum. Therefore, comparing the initial spectra with the filtered solution spectra yields information about the concentration and retention ability.

### Light intensity measurements

The light intensities were measured with the optical intensity handheld meter ML9002A (Anritsu). The silicone-based detector measured the total power incident onto the 9 mm-diameter circular surface of the probe.

### Thermal imaging

Thermal images were captured with the FLIR ONE infrared camera. It measured the intensity of infrared light (7.5 μm < λ < 14 μm) emitted by the objects in the field of view of the camera over an area of 160 by 120

pixels to compute their temperature. In the limit of sensibility of −20 °C to 120 °C the temperature resolution was of 0.1 °C.

### Colilert-18 test

The water sample/nutrient-indicator mixture was introduced into a Quanti-Tray (array of plastic reservoirs) and sealed with IDEXX Quanti-Tray Sealer. The sealed tray was placed in an incubator at 44.5 ± 0.2 °C for 18 h. The numbers of positive wells (yellow color) were translated into the Most Probable Numbers by a table provided with the trays.

### Throughput determination of viable bacteria by the colony-forming units (CFU) method

Evaluation of viable coliforms and *E. coli* in water samples was performed using the so-called colony-forming units (CFU) method. The CFU method is generally accepted for the evaluation and assessment of viable microorganisms, as well as for testing the impact of antimicrobial techniques and substances under various experimental conditions.

The initial concentration of *E. coli* bacteria used in this study was of 2–10<sup>8</sup> CFU/ml. All manipulations with the bacteria were performed using clean, sterile equipment, including pipette tips and Eppendorf tubes, solidified agar media, Petri dishes, and the bacterial cell spreader. To expose the *E. coli* bacteria in control experiments to UVA light, a UVA-light spot source, LC-8 Lightingcure™ (λ = 365 nm, 16 mW/cm<sup>2</sup>) from Hamamatsu Photonics (Japan) was used. In experiments aiming at characterizing the disinfecting potential of the filter material based on the TiO<sub>2</sub>NWs /CNTs nanocomposite, *E. coli* bacteria deposited on this filter were exposed to sunlight.

### ESR spectroscopy

The ESR experiments were carried out at room temperature using a cw-ESR X-band spectrometer, Bruker EleXsys E500 (Bruker BioSpin GmbH, Karlsruhe, Germany), equipped with a high-Q cylindrical cavity (Model ER 4122 SHQE). Water with 400 μM concentration of TEMPOL was passed through the filter and exposed to sunlight (as shown in Fig. 3) over a period of ~2.5 h. Small aliquots of about 20 μL were taken both before and after the filter at regular time intervals, transferred into 0.7 mm ID and 0.87 mm OD glass capillary tubes (VitroCom, NJ, USA), with a sample height of ca. 30 mm, and sealed on both ends with Cha-seal (Tube sealing compound, Chase Scientific Glass, Rockwood, TN, USA). The typical instrumental settings were: microwave frequency ~9.4 GHz; microwave power 0.633 mW; magnetic field sweep 120 G; magnetic field modulation frequency 100 kHz; magnetic field modulation amplitude 0.5 G; time constant 10.24 ms; spectral resolution 2048 points; conversion time 40.96 ms; resulting magnetic field sweeping time 84 s; two scans were accumulated per one trace. To evaluate the number of spins in the individual samples, the respective ESR spectra were double-integrated using a software tool (OriginPro2019) and the obtained signal intensities were compared with the intensity of the reference signal (400 μM TEMPOL).

### Photodegradation of Methyl orange—a UV–VIS assay

Methyl orange solution (MO) with an initial concentration of 20 mg/L was poured into Petri dishes containing the test samples in the form of discs (50 mm in diameter) at their bottom. For the purpose of exposure to UVA light, a UV spot light source, LC-8 Lightingcure™ (λ<sub>exc</sub> = 365 nm, 16 mW/cm<sup>2</sup>), from Hamamatsu Photonics (Japan), was used. The photodegradation of the dye and the corresponding changes in its concentration were monitored by measuring the characteristic MO absorbance peak at 464 nm with a UV–Vis spectrophotometer, Varian Cary 50, Agilent (USA). In order to obtain the time dependencies, small aliquots (2.5 mL) were taken every 10 min from Petri dishes and transferred to the cuvettes of the UV–VIS spectrophotometer.

### DATA AVAILABILITY

The data that support the findings of this study are available from the corresponding author upon reasonable request.

Received: 3 October 2021; Accepted: 11 March 2022;

Published online: 07 April 2022

## REFERENCES

- Progress on Drinking Water, Sanitation and Hygiene: 2017 Update and SDG Baselines. Geneva: World Health Organization (WHO) and the United Nations Children's Fund (UNICEF), 2017. Licence: CC BY-NC-SA 3.0 IGO
- <https://www.unicef.org/reports/progress-drinking-water-sanitation-and-hygiene>
- Matsunaga, T. et al. Photoelectrochemical sterilization of microbial cells by semiconductor powders. *FEMS Microbiol. Lett.* **29**, 211–214 (1985).
- Duff, W. S. & Hodgson, D. A. A simple high efficiency solar water purification system. *Sol. Energy* **79**, 25–32 (2005).
- Gumy, D. et al. Solar photocatalysis for detoxification and disinfection of water: different types of suspended and fixed TiO<sub>2</sub> catalysts study. *Sol. Energy* **80**, 1376–1381 (2006).
- Matthews, R. W. Solar-electric water purification using photocatalytic oxidation with TiO<sub>2</sub> as a stationary phase. *Sol. Energy* **38**, 405–413 (1987).
- McCullagh, C. et al. The application of TiO<sub>2</sub> photocatalysis for disinfection of water contaminated with pathogenic micro-organisms: a review. *Res. Chem. Intermed.* **33**, 359–375 (2007).
- Reddy, P. V. L. et al. TiO<sub>2</sub>-based photocatalytic disinfection of microbes in aqueous media: a review. *Environ. Res.* **154**, 296–303 (2017).
- Nakata, K. & Fujishima, A. TiO<sub>2</sub> photocatalysis: design and applications. *J. Photochem. Photobiol. C. Photochem. Rev.* **13**, 169–189 (2012).
- Chen, D. & Ray, A. K. Photodegradation kinetics of 4-nitrophenol in TiO<sub>2</sub> suspension. *Water Res.* **32**, 3223–3234 (1998).
- Chatterjee, D. & Mahata, A. Demineralization of organic pollutants on the dye modified TiO<sub>2</sub> semiconductor particulate system using visible light. *Appl. Catal. B* **33**, 119–125 (2000).
- Matsusawa, S. et al. Immobilization of TiO<sub>2</sub> nanoparticles on polymeric substrates by using electrostatic interaction in the aqueous phase. *Appl. Catal. B* **83**, 39–45 (2008).
- Wood, D. et al. An overview of photocatalyst immobilization methods for air pollution remediation. *Chem. Eng. J.* **391**, 1–16 (2020).
- Arora, B. & Attri, P. Carbon Nanotubes (CNTs): a potential nanomaterial for water purification. *J. Compos. Sci.* **4**, 1–33 (2020).
- Naffati, N. et al. Carbon-nanotube/TiO<sub>2</sub> materials synthesized by a one-pot oxidation/hydrothermal route for the photocatalytic production of hydrogen from biomass derivatives. *Mater. Sci. Semicond. Process.* **115**, 1–7 (2020).
- Tétrault, N. et al. High-efficiency solid-state dye-sensitized solar cells: fast charge extraction through self-assembled 3D fibrous network of crystalline TiO<sub>2</sub> nanowires. *ACS Nano* **2**, 7644–7650 (2010).
- Hernadi, K. et al. Synthesis of MWNT-based composite materials with inorganic coating. *Acta Materialia* **51**, 1447–1452 (2003).
- Paiva, C. N. & Bozza, M. T. Are reactive oxygen species always detrimental to pathogens? *Antioxid. Redox Signal.* **20**, 1000–1037 (2014).
- Horváth, E. et al. Photocatalytic Nanowires-Based Air Filter: Towards Reusable Protective Masks. *Adv. Funct. Mater.* **30**, 2004615 (2020).
- Horváth, E., Forró, L. & Magrez, A. Titanium oxide aerogel composites, US Patent No. US2016030908 (A1)
- Smajda, R. et al. Production of high quality carbon nanotubes for less than \$1 per gram. *Phys. Status Solidi (C)* **7**, 1236–1240 (2010).
- Osada, Y. & Nakagawa, T. Membrane science and technology. Edited by Marcel Dekker Inc., New York, 1992.
- Marshall, D. I. et al. Oxidation of 4-substituted TEMPO derivatives reveals modifications at the 1- and 4-positions. *Org. Biomol. Chem.* **9**, 4936–4945 (2011).
- Lu, H. et al. Superoxide dismutase mimetic drug tempol aggravates anti-GBM antibody-induced glomerulonephritis in mice. *Am. J. Physiol. Ren. Physiol.* **299**, 445–452 (2010).
- Wilcox, C. S. Effects of tempol and redox-cycling nitroxides in models of oxidative stress. *Pharmacol. Ther.* **126**, 119–145 (2010).
- Saito, K. et al. Two reaction sites of a spin label, TEMPOL (4-hydroxy-2, 2, 6, 6-tetramethylpiperidine-N-oxyl), with hydroxyl radical. *J. Pharm. Sci.* **92**, 275–280 (2003).
- Marshall, D. I. et al. Oxidation of 4-substituted TEMPO derivatives reveals modifications at the 1- and 4-positions. *Org. Biomol. Chem.* **9**, 4936–4947 (2011).
- Yan, S. C., Li, Z. S. & Zou, Z. G. Photodegradation of Rhodamine B and Methyl Orange over Boron-Doped g-C<sub>3</sub>N<sub>4</sub> under Visible Light Irradiation. *Langmuir* **26**, 3894–3901 (2010).
- Wang, J. et al. Preparation of zinc tungstate nanomaterial and its sonocatalytic degradation of meloxicam as a novel sonocatalyst in aqueous solution. *Ultrason Sonochem.* **18**, 177–183 (2011).
- Gómez-Obando, V. A. et al. CWPO degradation of methyl orange at circumneutral pH: multi-response statistical optimization, main intermediates and by-products. *Front. Chem.* **7**, 1–15 (2019).
- DiPaola, A. et al. Heavy metal removal from water/wastewater by nanosized metal oxides: a review. *J. Hazard. Mater.* **211**, 3–29 (2012).
- Baby, R. et al. Carbon nanomaterials for the treatment of heavy metal-contaminated water and environmental remediation. *Nanoscale Res. Lett.* **14**, 341–349 (2019).
- Gonsioroski, A., Mourikes, V. E. & Flaws, J. A. Endocrine disruptors in water and their effects on the reproductive system. *Int. J. Mol. Sci.* **21**, 1–66 (2020).
- Damalas, C. A. & Eleftherohorinos, I. G. Pesticide exposure, safety issues, and risk assessment indicators. *Int. J. Environ. Res. Public Health* **8**, 1402–1419 (2011).
- Patel, M. et al. Pharmaceuticals of emerging concern in aquatic systems: chemistry, occurrence, effects, and removal methods. *Chem. Rev.* **119**, 3510–3673 (2019).
- Edberg, S. C., Allen, M. J., Smith, D. B. & Kriz, N. J. Enumeration of total coliforms and escherichia coli from source water by the defined substrate technology. *Appl. Environ. Microbiol.* **56**, 366–369 (1990).
- Geissmann, Q. OpenCFU, a new free and open-source software to count cell colonies and other circular objects'. *PLoS one* **8**, 11–110 (2013).
- Bucharskaya, A. et al. Towards effective photothermal/photodynamic treatment using plasmonic gold nanoparticles. *Int. J. Mol. Sci.* **17**, 1295–1301 (2016).
- Guerrero-Florez, V. et al. Gold nanoparticle-mediated generation of reactive oxygen species during plasmonic photothermal therapy: a comparative study for different particle sizes, shapes, and surface conjugations. *J. Mater. Chem. B* **8**, 2862–2875 (2020).
- Yang, X. et al. The use of tunable optical absorption plasmonic Au and Ag decorated TiO<sub>2</sub> structures as efficient visible light photocatalysts. *Catalysts* **10**, 1–14 (2020).
- Richardson, H. H. et al. Thermo-optical properties of gold nanoparticles embedded in ice: characterization of heat generation and melting. *Nano Lett.* **6**, 783–788 (2006).
- Garnett, E. & Yang, P. D. Light trapping in silicon nanowire solar cells. *Nano Lett.* **10**, 1082–1087 (2010).
- Chen, X. et al. Broadband enhancement in thin-film amorphous silicon solar cells enabled by nucleated silver nanoparticles. *Nano Lett.* **12**, 2187–2192 (2012).
- Feng, N. N. et al. Design of highly efficient light-trapping structures for thin-film crystalline silicon solar cells. *IEEE T Electron Dev.* **54**, 1926–1933 (2007).
- Dewan, R. et al. Light trapping in thin-film silicon solar cells with submicron surface texture. *Opt. Express* **17**, 23058–23065 (2009).
- Couteau, E. et al. CVD synthesis of high-purity multiwalled carbon nanotubes using CaCO<sub>3</sub> catalyst support for large-scale production. *Chem. Phys. Lett.* **378**, 9–17 (2003).
- Seo, J. W. et al. Synthesis and manipulation of carbon nanotubes. *N. J. Phys.* **5**, 120.1–120.22 (2003).

## ACKNOWLEDGEMENTS

E.H. gratefully acknowledges the Global Water Award of the United Arab Emirates, the Swiss-South African collaboration grant, and the support of the Karl Zeno Schindler Foundation. We would also like to thank Lenke Horváth and Rita Smajda, for their assistance in the early stage of the experiments.

## AUTHOR CONTRIBUTIONS

E.H. was the project leader and synthesized the materials. L.R. did the electron microscopy. J.G. worked with the prototype and characterized the filter paper with G.B., E.V.-R. and M.B.-M. The micropollutant test was performed by M.G., D.G. and F.B. The ESR measurements were done by A.S. who has participated in the paper writing. L.F. is the team leader and wrote the paper. All authors approved the manuscript.

## COMPETING INTERESTS

The authors declare no competing interests.

## ADDITIONAL INFORMATION

**Correspondence** and requests for materials should be addressed to E. Horváth or L. Forró.

**Reprints and permission information** is available at <http://www.nature.com/reprints>

**Publisher's note** Springer Nature remains neutral with regard to jurisdictional claims in published maps and institutional affiliations.



**Open Access** This article is licensed under a Creative Commons Attribution 4.0 International License, which permits use, sharing, adaptation, distribution and reproduction in any medium or format, as long as you give appropriate credit to the original author(s) and the source, provide a link to the Creative Commons license, and indicate if changes were made. The images or other third party material in this article are included in the article's Creative Commons license, unless indicated otherwise in a credit line to the material. If material is not included in the article's Creative Commons license and your intended use is not permitted by statutory regulation or exceeds the permitted use, you will need to obtain permission directly from the copyright holder. To view a copy of this license, visit <http://creativecommons.org/licenses/by/4.0/>.

© The Author(s) 2022